Retrofitting of steel T-Joints by Plasma and Tungsten Inert Gas dressing

Ramalho, A.L.[1,2]

[1]Polytechnic Institute of Castelo Branco, 6000-767 Castelo Branco, Portugal

[2]CEMMPRE, Department of Mechanical Engineering, University of Coimbra, 3004-516 Coimbra, Portuga

Summary

- Introduction
- Experimental Procedure
- Numerical Model
- Results Discussion
- Conclusions

Introduction

- Economic and environmental constrains promotes prolonging the life of welded structures;
- Additional effort is required in inspection, monitoring and rehabilitation of damaged details;
- The main cause of damage is the growth of fatigue cracks at the weld toe of the joints;
- Plasma and TIG remelting are efficient repair techniques of pre-cracked welded joints;
- In this communication is presented the main results of the work developed by the author, relevant to assess the efficiency of sustainable repair, by Plasma and TIG remelting, of steel welded structures.

Experimental Procedure – Materials

Chemical composition of used S355 AR steel (wt %).

C	Si	Mn	Cr	Mo	Ni	Ti
0.131	0.413	1.44	0.063	0.024	0.034	0.009
Al	V	Cu	Co	Nb	P	S
0.029	0.043	0.018	0.013	0.005	0.011	0.005

The base material was a medium strength steel, S355, in the form of plates with 12.5 mm of thickness.

Tensile test at ambient temperature:

- The mechanical properties of the base material were obtained using the procedure defined in the tensile test European standard (EN 10002-1).

Tensile test at high temperature:

- The mechanical properties variation with temperature of the S355 AR steel, were obtained through tensile tests carried out at temperatures of 18, 150, 300, 450, 525 and 600°C;
- The tests were carried out using an Instron servo-hydraulic machine (EN 10002-5);
- Were used an axial strain gauge, model Instron-A1387-1023, coupled directly to the specimen.

Experimental Procedure – Materials

- The thermal expansion coefficient was obtained through thermomechanical analysis;
- Were tested three cylindrical samples;
- A nitrogen flow of 60 ml/minute and a heating rate of 10°C/minute was used;
- The thermal expansion coefficient was obtained for temperatures between 40 and 1350°C, being obtained at every increase of 10°C;
- The specific heat was obtained through differential scanning calorimetry;
- Three cylindrical samples, were tested;
- The specific heat was obtained for temperatures between 400 and 950°C, being obtained at each variation of 2.5°C.

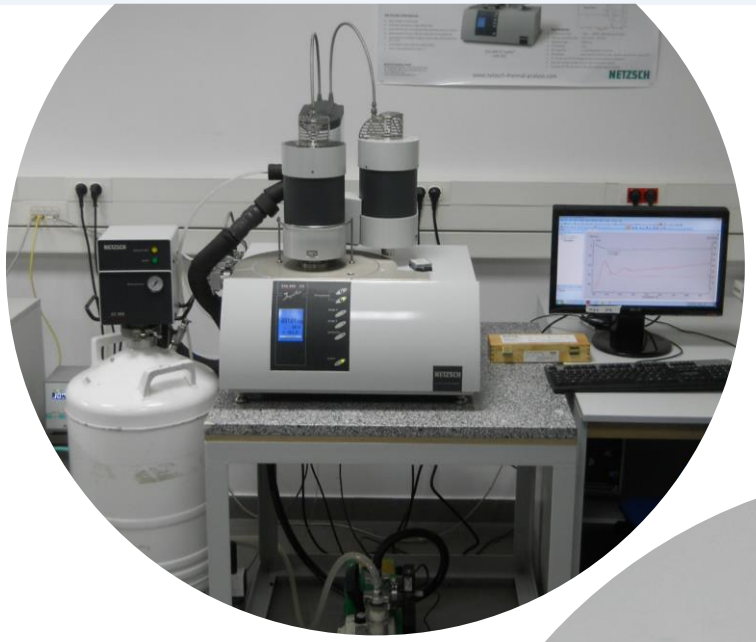

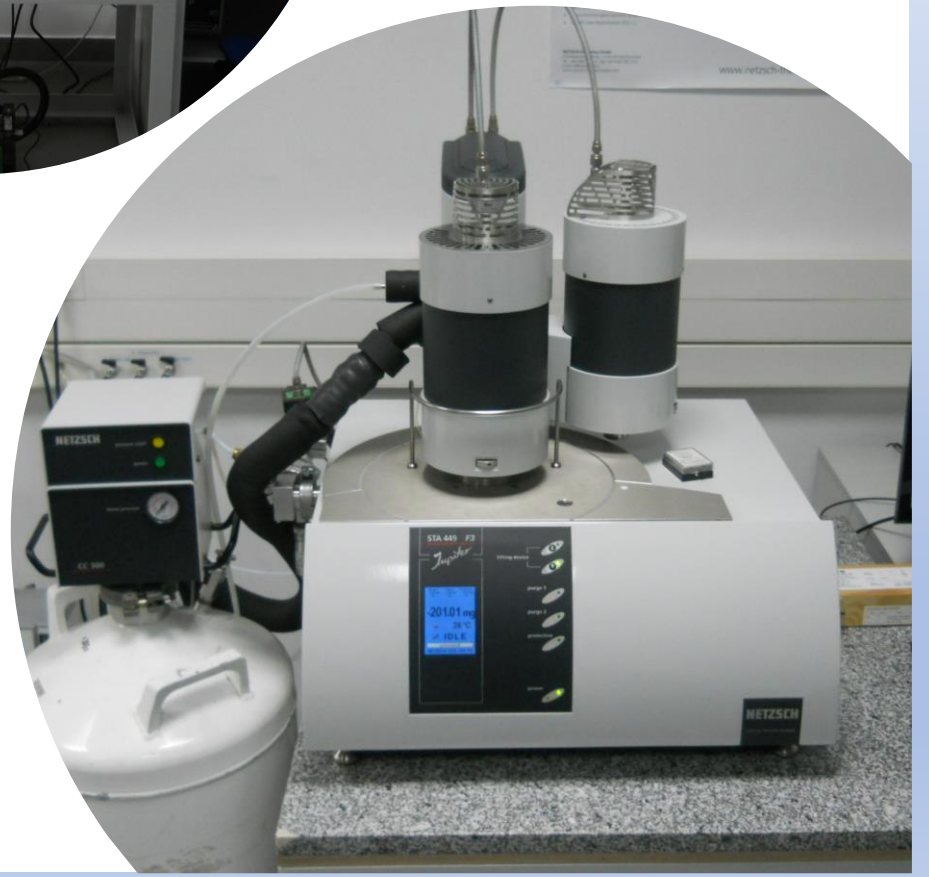

Experimental Procedure – T-Welded Specimens

Chemical composition of weld metal (wt %).

C	Si	Mn	Cr	Ni	Mo	P	S
0.08	0.45	1.28	0.5	1.87	0.37	0.017	0.01

- The welds were made by covered electrode (ESAB OK 75.75) process with weld metal in overmatching condition;
- T-joints weld specimens were produced from the main plates with low penetration fillet;
- For the specimens of TAS series, a TIG dressing improvement treatment are applied at the weld toe.

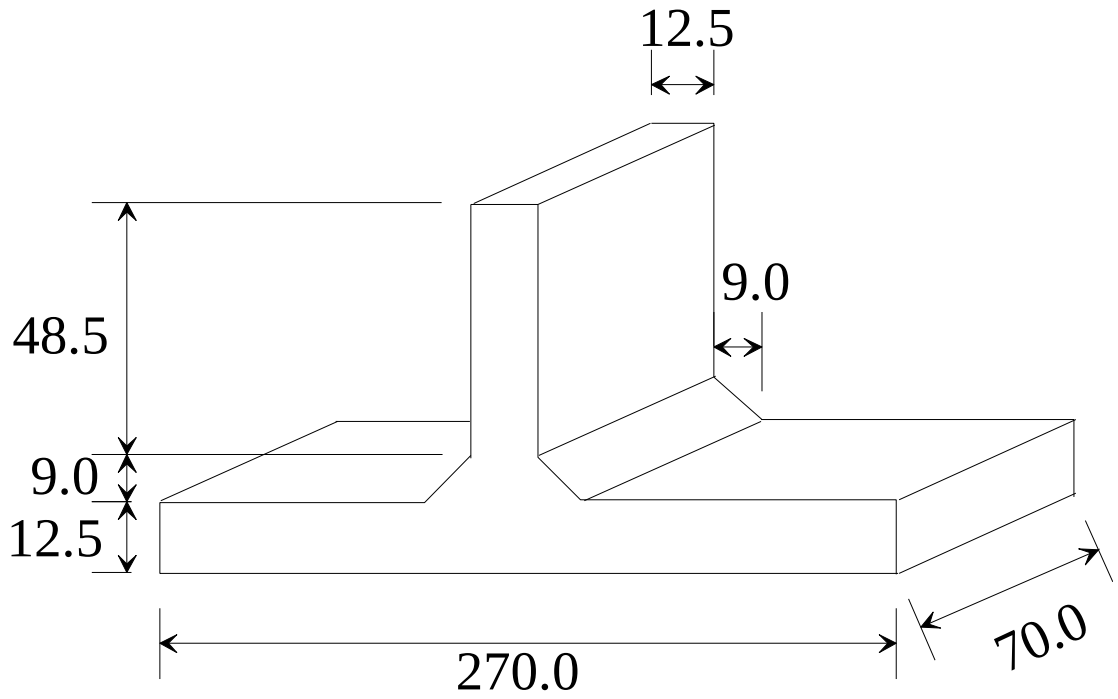

Experimental Procedure – Fatigue and Repair

- The T-joints were loaded in three-point bending fatigue until generating visible cracks at the weld toe for the specimens of series TDR and PDR, and to the rupture for the AW and TAS series;
- For the TDR series, TIG repair was performed at the weld toe;
- For the PDR series, Keyhole plasma repair was performed at the weld toe;
- For the TR-D series, to detect the initiation and propagation of fatigue cracks from the weld toe it was used the strain gauge method technique, and the repair was done when the cracks remained shallow.

TIG dressing (TDR)	Deeper TIG dressing (TR-D)	Plasma keyhole dressing (PDR)
Argon flux; Current intensity 110 A; Tension DC 19 V; Linear rate 1.08 mm/s.	Argon flux; Current intensity 135 A; Tension DC 15 V; Linear rate 0.66 mm/s.	Argon flux; Current intensity 200 A; Tension DC 30 V; Linear rate 2.47 mm/s.

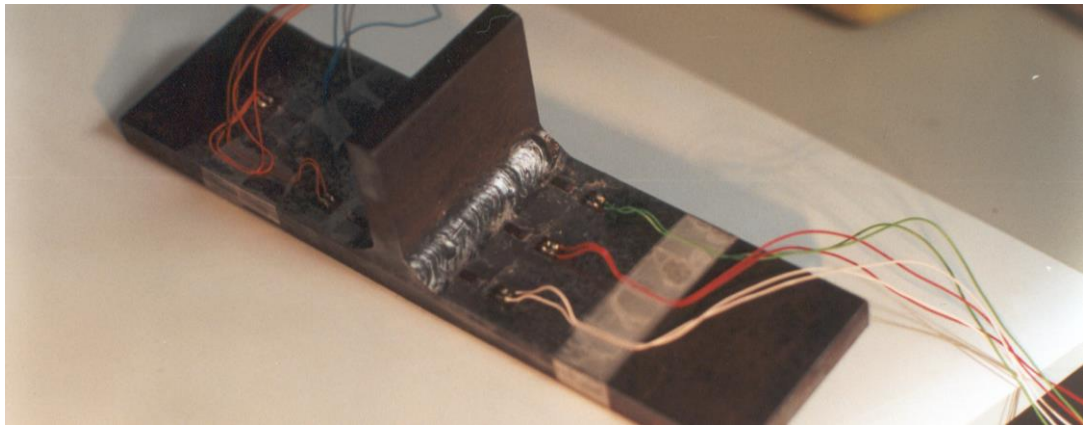

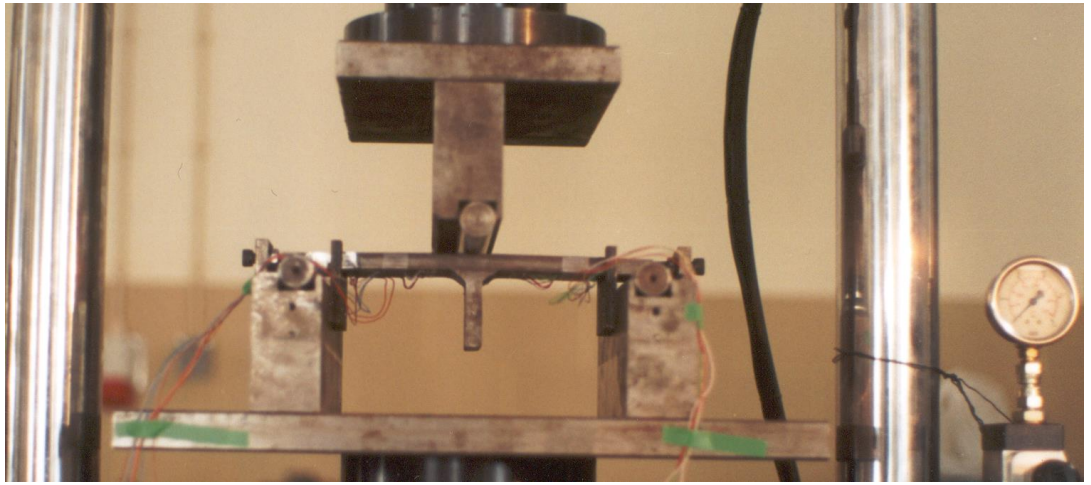

Numerical Model

- It was assumed symmetry conditions in the middle plane and only half of the specimens was considered;
- The numerical models were developed using the software MSC Marc and the MSC Patran mesher;
- To simulate the welding residual stress field, it was assumed that the influence of deformation and the thermodynamic effects of microstructural changes have despicable effect in the thermal analysis;
- The simulation was carried out in a sequentially coupled analysis: a thermal analysis was followed by a structural analysis;
- The fatigue crack propagation on the weld toe, considering the effect of the welding residual stress field, were simulated by integration of the Paris-Erdogan low, using the virtual crack closure technique (VCCT);
- The mesh consists of tetrahedral full integration linear elements;
- The numerical models were run under a windows server 2016 virtual server, Intel Xeon dual processor, with 128 Gb of RAM.

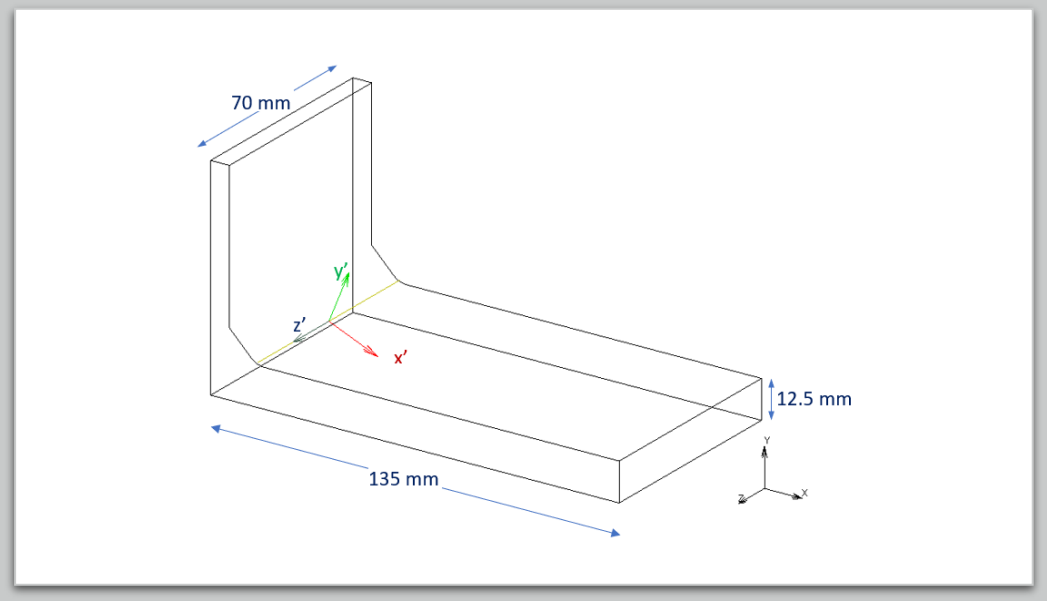

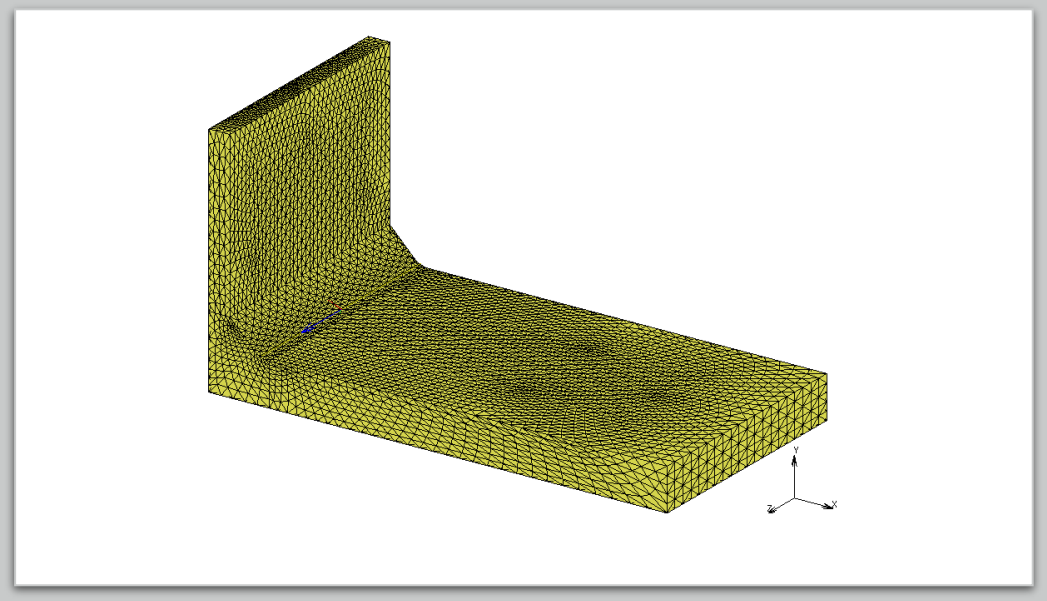

Numerical Model – Heat transfer analysis

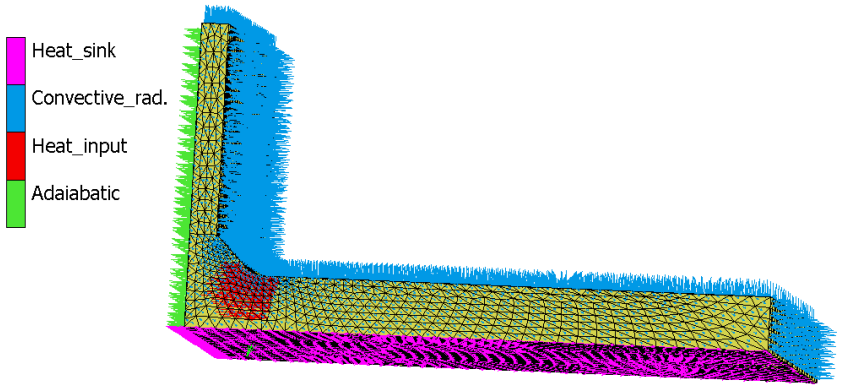

- A 3D transient non-linear heat flow finite element analysis was performed;
- **Adiabatic boundary conditions** were considered in the symmetry plane, in the base of the specimen was considered a heat sink as a **fixed temperature boundary** and in all the other surfaces, **convective-radiative** conditions were used;
- For the convective and radiative boundary conditions, a combined heat transfer coefficient was calculated using the equation:

  $h=24.1x10^{-4}\varepsilon T^{1.61}$ where T unit is °C, h unit is Wm^{-2} $°C^{-1}$ and ε is the emissivity of the surface of the body that assumed the value of 0.9;

- The variation of the thermal conductivity with the temperature was obtained from literature for similar materials;
- A latent heat of fusion of 247 $kJkg^{-1}$ was assumed to be absorbed/released between the solidus and liquidus temperatures;
- The heat generated by the arc welding was inputted using the **double ellipsoid heat source** model:

$$q(x',y',z'',t) = \frac{6\sqrt{3}f\ Q}{abc\pi\sqrt{\pi}}\ e^{-3x'^2/a^2}\ e^{-3y'^2/b^2}\ e^{-3z'^2/c^2}$$

where Q is the het input, Q=ηVI, η is the efficiency of the weld process, V is the voltage, and I the amperage, it was assumed an efficiency of η=0.6, tor TDR series, V= 110 V, I= 22 A, for the frontal semi-ellipsoid f=0.6, $c=c_1$=3 mm, a=2.4 mm and b=1.4 mm, and for the rear semi-ellipsoid f=1.4 $c=c_2$=6 mm.

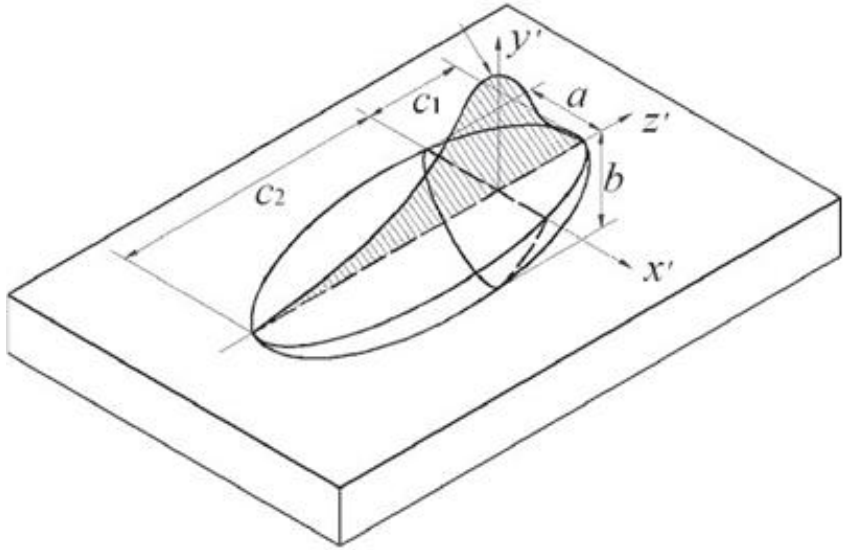

Numerical Model – Structural analysis

- A 3D quasi-static structural analysis was carried out with the same mesh that was used in the thermal analysis;
- In the symmetry plane horizontal displacement restriction was performed and in the upper nodes on the right side, springs, with despicable stiffness, were added, in order to restrict the rigid body motion;
- The material was modelled as elasto-plastic, with a rate independent von Mises plasticity, using a combined hardening rule;
- Were used temperature-dependent mechanical properties for Young modulus, Poisson ratio, Yield stress and hardening modulus;
- The loading was performed, with a state variable boundary condition, by gradually imposing the deformation field originated by the temperature fields obtained in the preceding thermal analysis.

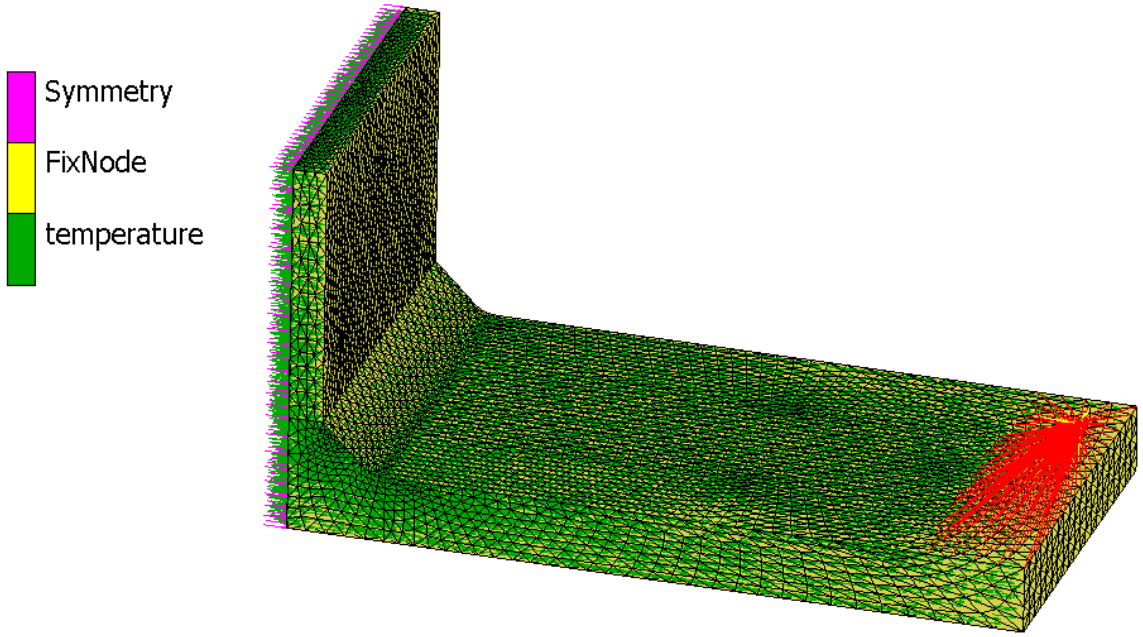

Numerical Model – Crack generation

- In the initial mesh is generated a semi-elliptical pre-existing crack: for TR-D specimen, with 0,5 mm of depth and a superficial length of 2 mm and for TDR3 specimen the crack is embedded, being 3.3 mm deep and having a length of 30 mm;
- This initial crack is generated in MSC Marc software by a faceted surface, through a remeshing process.

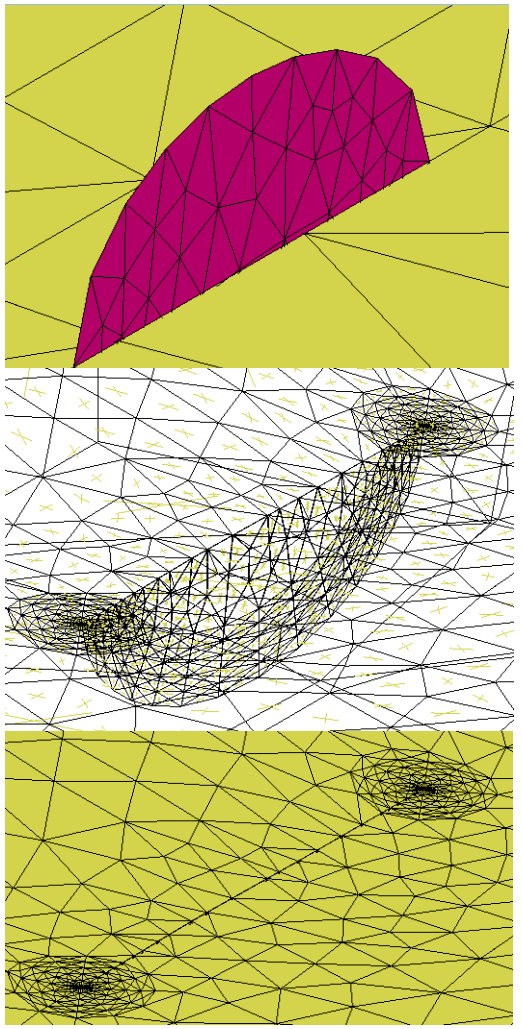

Numerical Model – Fatigue crack loading

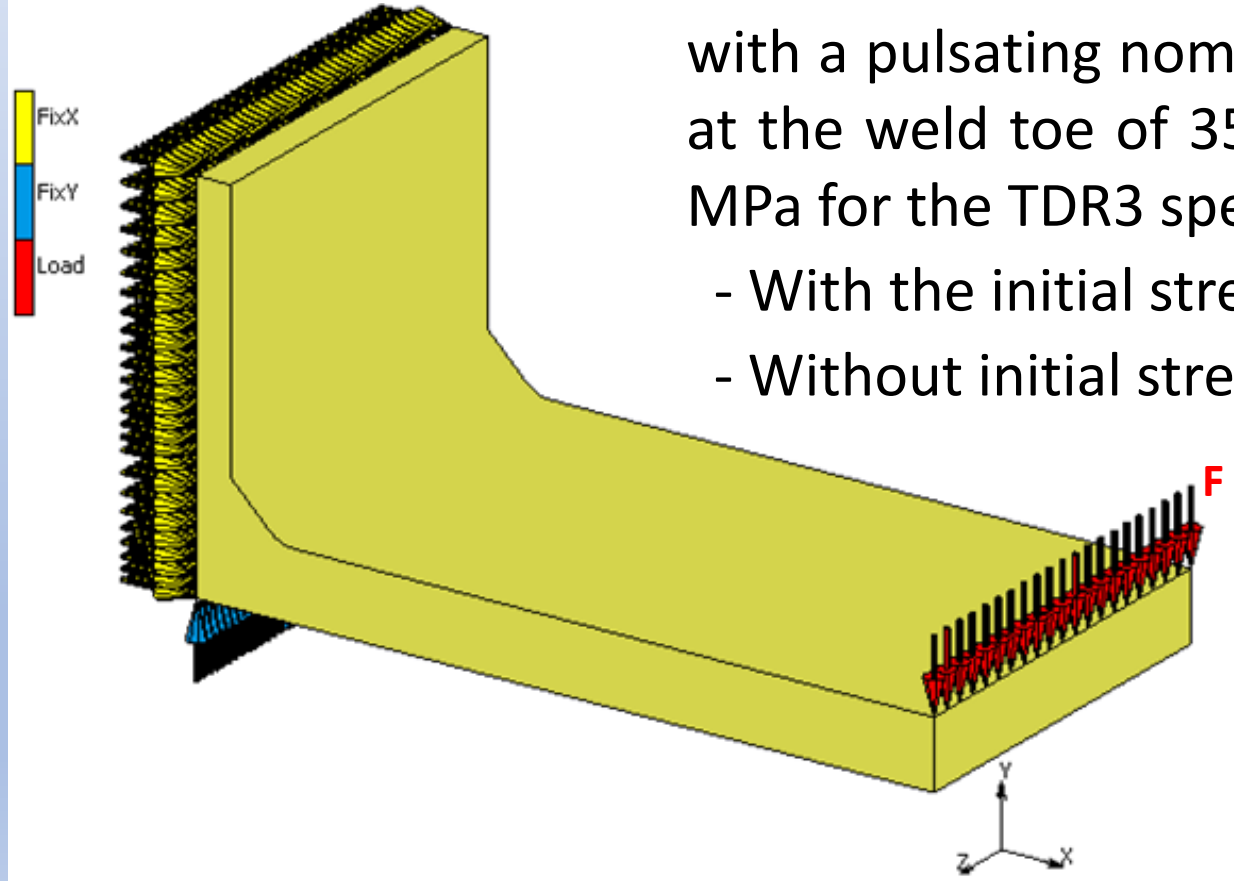

- This model will be subjected to three-point bending fatigue, with a pulsating nominal load, F, corresponding to a stress range at the weld toe of 352.6 MPa for the TR-D specimen and 204.7 MPa for the TDR3 specimen, in two different initial conditions:
  - With the initial stress field previously estimated;
  - Without initial stress field.

Numerical Model – Fatigue crack propagation

- The crack's propagations were evaluated using the integration of the Paris-Erdogan law, according to:

$$\Delta a = \int_{a_i}^{a_f} da = \int_{N_i}^{N_f} C\Delta K^m \, dN.$$

- For the material propagation constants were used the values, C = 1.2288×10^{-8} and m= 2.6, with da/dN in mm/cycle and K in $MPa.m^{1/2}$;
- The stress intensity factors were obtained using the 3D VCCT technique implemented in MSC Marc software;
- It was used a maximum crack growth increment of Δa_0 = 1.1 mm.

Results Discussion – Experimental Analysis

- The mechanical properties obtained in the tensile tests at room temperature, for the base material were presented in table A;
- The variation of yield stress and hardening modulus with temperature are presented in table B;
- From the analysis of the results presented in table B, were observed the increasing of hardening modulus up to 450 °C;
- From 450°C to 600°C, there is a significant decrease in stiffness and strength, and were observed the decrease of hardening modulus.

Table A Mechanical Properties for the S355 AR steel (room temperature).

Specimen	ε_R [%]	σ_R [MPa]	$\varepsilon_{0.2}$ [%]	$\sigma_{0.2}$ [MPa]	E [MPa]
1	20.95	554.4	0.3074	386.7	228000
2	19.94	558.0	0.3597	367.0	184000
4	26.64	553.9	0.3423	393.6	223800
5	22.59	554.5	0.3812	387.3	215300
Average	**22.53**	**555.2**	**0.3476**	**383.7**	**212800**
Standard deviation	**2.95**	**1.89**	**0.03**	**11.53**	**17231.71**

Table B Mechanical Properties for the S355 AR steel (high temperature).

T [°C]	$\sigma(\varepsilon_p=0)$ [MPa]	$\sigma(\varepsilon_p=0.023)$ [MPa]	$\sigma(\varepsilon_p=0.047)$ [MPa]	$\sigma(\varepsilon_p=0.057)$ [MPa]	$\sigma(\varepsilon_p=0.17)$ [MPa]
18	383.7	484.4	541.2	551.7	551.7
150	368.0	432.3	502.1	515.3	515.3
300	367.1	463.5	520.0	523.4	523.4
450	338.4	496.3	554.3	563.5	-
525	289.3	433.1	480.8	486.0	-
600	238.0	283.1	289.3	289.3	-

Results Discussion – Experimental Analysis

- The picture shows the variation of the linear and unitary coefficient of thermal expansion (α) for the S355 steel;
- In picture are superposed the values proposed by Eurocode for a steel with similar chemical composition;
- From the presented data, it can be seen that the values proposed by Eurocode 3 are very close to the experimental data.

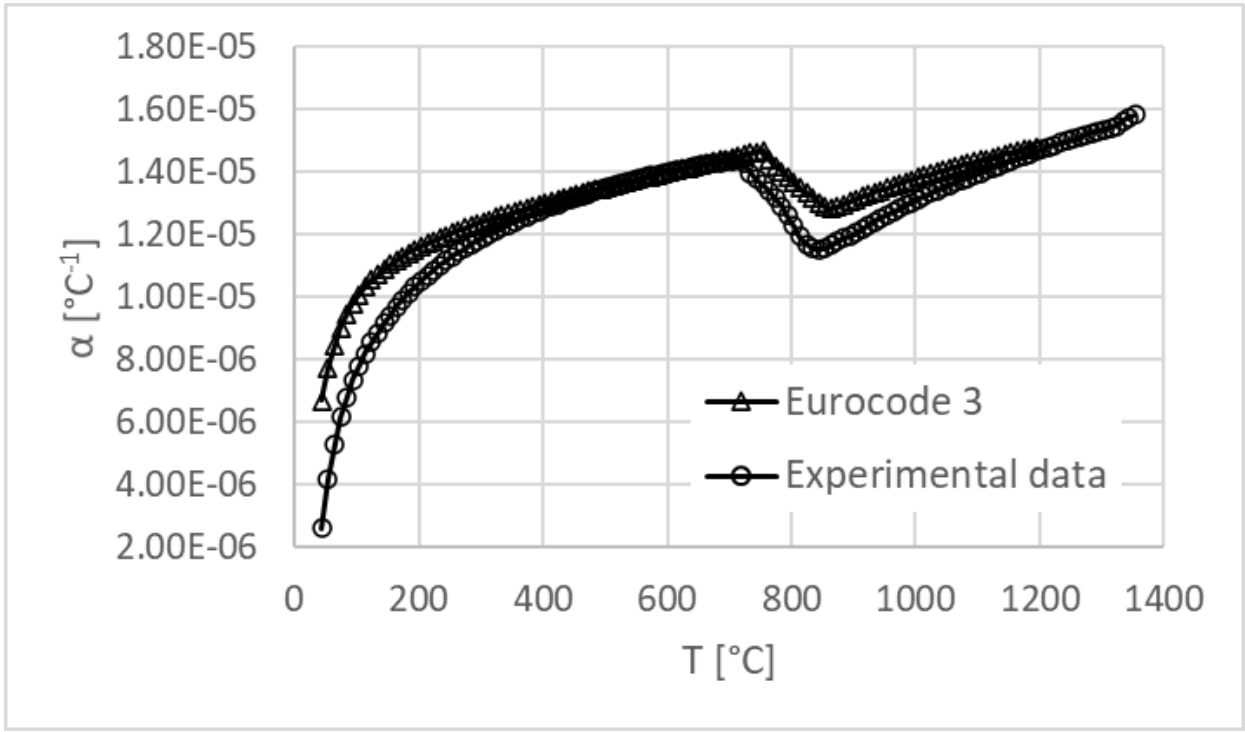

Results Discussion – Experimental Analysis

- The picture shows the variation of specific heat (Cp) for S355 AR steel;
- In picture are superposed the values proposed by Eurocode for a steel with similar chemical composition;
- The obtained values for the variation of specific heat with temperature, follow a trend close to that proposed by Eurocode 3.

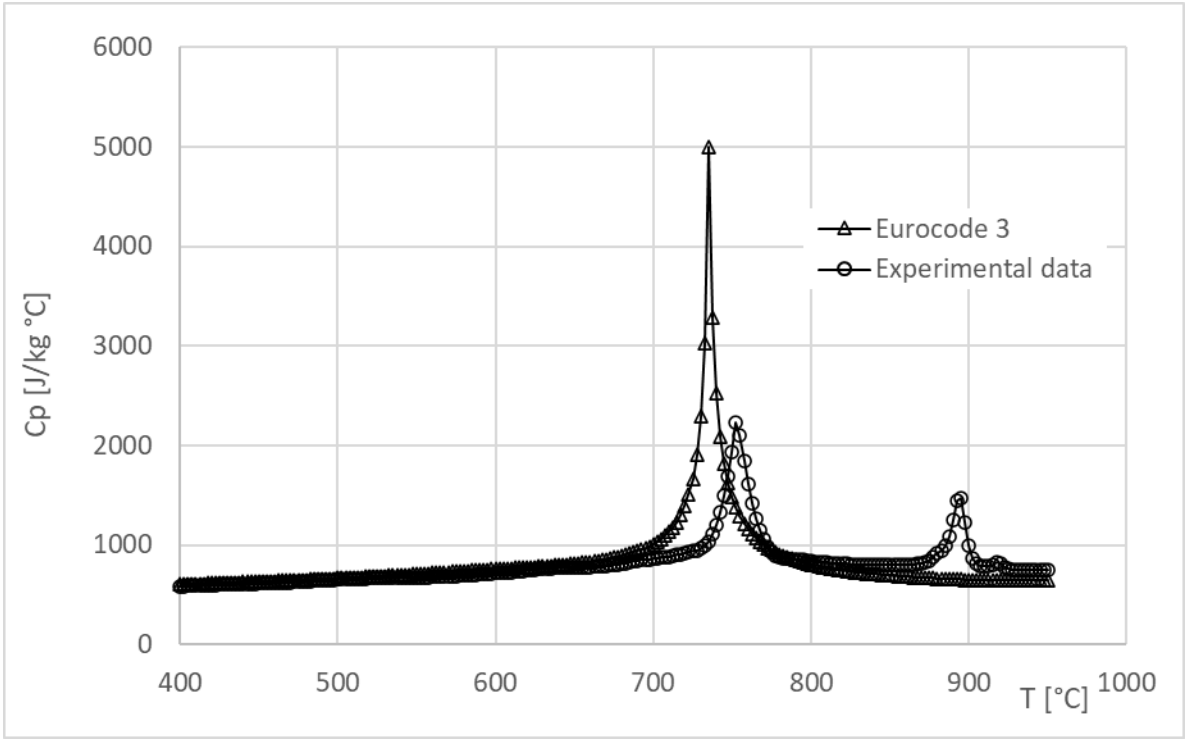

Results Discussion – Experimental Analysis

- In picture are presented the experimental points obtained for the fatigue tests and the S–N curves for the AW, TAS, TDR and PDR series;
- Fatigue results were fitted by using the equation:

$$\Delta\sigma = KN_r^m$$

where $\Delta\sigma$ is the nominal stress range at the weld toe, N_r is number of cycles to failure, K and m are constant parameters;

- The best fit parameters obtained by linear regression are indicated in the picture.

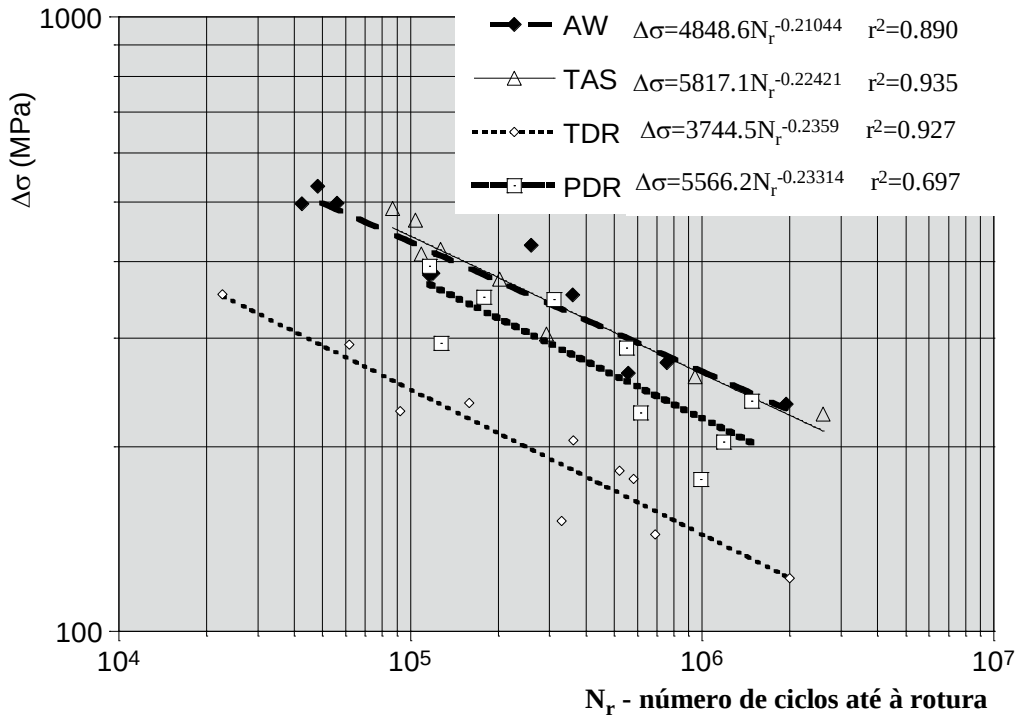

Results Discussion – Experimental Analysis

The fatigue results for TDR series are presented in the table. For comparison purposes, in the tables are presented the lives obtained by the S-N curve for the AW Serie, designated by $N_{AW\ S\text{-}N}$;

The fracture surfaces of the specimens are also presented.

From the presented results we can draw the following considerations:

- The rehabilitation of deep fatigue cracks at the weld toe (a_r greater than 4 mm) by TIG dressing, leads to very small post-repair fatigue lives (varies from 4% to 10%), when compared to the lives of as welded specimens;
- The TIG remelting have a small penetration (lesser than 1.75 mm;
- The TIG remelting is not suitable to promote the repair of deep cracks.

Specimen	a_r [mm]	$\Delta\sigma$ [MPa]	N_r	$N_{AW\ S\text{-}N}$	Fracture surface
TDR1	6.50	354.2	22680	251134	
TDR2	5.10	151.2	329711	14343932	
TDR3	4.80	204.7	361890	3400004	
TDR4	5.40	122.0	1998624	39765559	
TDR5	5.90	143.9	691645	18146433	
TDR6	4.70	235.5	159236	1746694	
TDR7	4.83	293.3	61808	615546	
TDR8	4.35	182.8	521075	5820975	
TDR9	4.72	177.1	582198	6766601	
TDR10	6.90	228.1	92327	2095975	

Results Discussion – Experimental Analysis

From the fatigue results for the TR-D series, presented in the table, we can draw the following considerations:

- The rehabilitation of shallow fatigue cracks at the weld toe (a_r lesser than 2.5 mm) by TIG dressing, leads to higher post-repair fatigue life (245%), when compared to the life of as welded specimens;
- The welding parameters used for the TR-D series leads to higher penetration of TIG remelting;
- The TIG remelting is suitable to promote the repair of shallow cracks;
- The use of TIG remelting as a fatigue crack repair technique, must be associated with an adequate monitoring technique to ensure that the repair is carried out at an early stage of propagation, when the cracks are still shallow.

Specimen	a_r [mm]	$\Delta\sigma$ [MPa]	N	$N_{AW\ S\text{-}N}$	Fracture surface
TR-D	<2.5	352.6	628739	256596	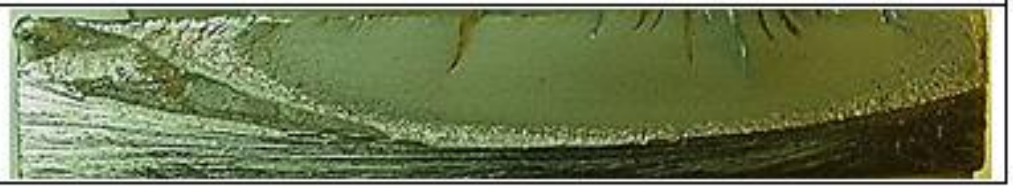

Results Discussion – Experimental Analysis

From the fatigue results for PDR series, presented in the table, we can draw the following considerations:

- The rehabilitation of deep fatigue cracks at the weld toe (a_r varying from 2.2 to 5.9 mm) by keyhole plasma, leads to small post-repair fatigue lives, when compared to the lives of as-welded specimens;
- The lives obtained for the PDR5 to PDR9 specimens vary from 67% to 112% of the as welded ones, but for the remaining specimens are much lower (14% to 34%);
- The results have a great scatter, but it can be drawn that keyhole plasma promotes a reasonable repair of deep cracks;
- However, a very high porosity density is observed, this porosity is not acceptable for most applications, being rejected by welding codes
- For this reason, despite the increased penetration, the use of the plasma or TIG in keyhole variants do not prove to be suitable to promote the repair of fatigue cracks generated in welded joints.

Specimen	a_r [mm]	$\Delta\sigma$ [MPa]	N	N_{AWS-N}	Fracture surface
PDR1	2.20	203.4	1185720	3504512	
PDR2	5.18	176.6	988050	6858123	
PDR3	4.83	226.7	615786	2093198	
PDR4	5.43	294.4	127110	604693	
PDR5	4.74	289.1	550079	659213	
PDR6	5.90	346.5	311338	278782	
PDR7	5.06	349.8	178495	266504	
PDR8	3.63	237.1	1482055	1691387	
PDR9	5.80	393.0	116388	153245	

Results Discussion – Numerical analysis

- The estimated residual stresses were compared with experimental results;
- This numerical model was validated by the obtained good agreement between the numerical predictions and experimental values obtained by X-ray diffraction and hole drilling technique;
- The estimated residual stress field was computed as initial conditions in the crack growth process.

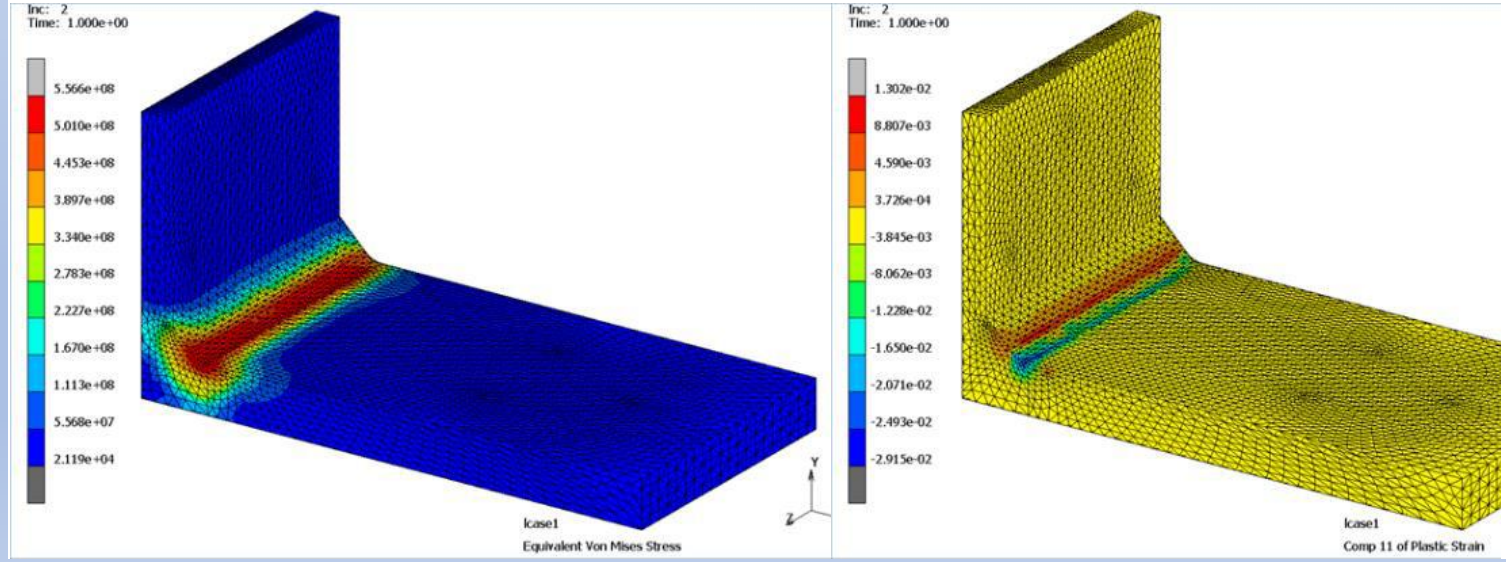

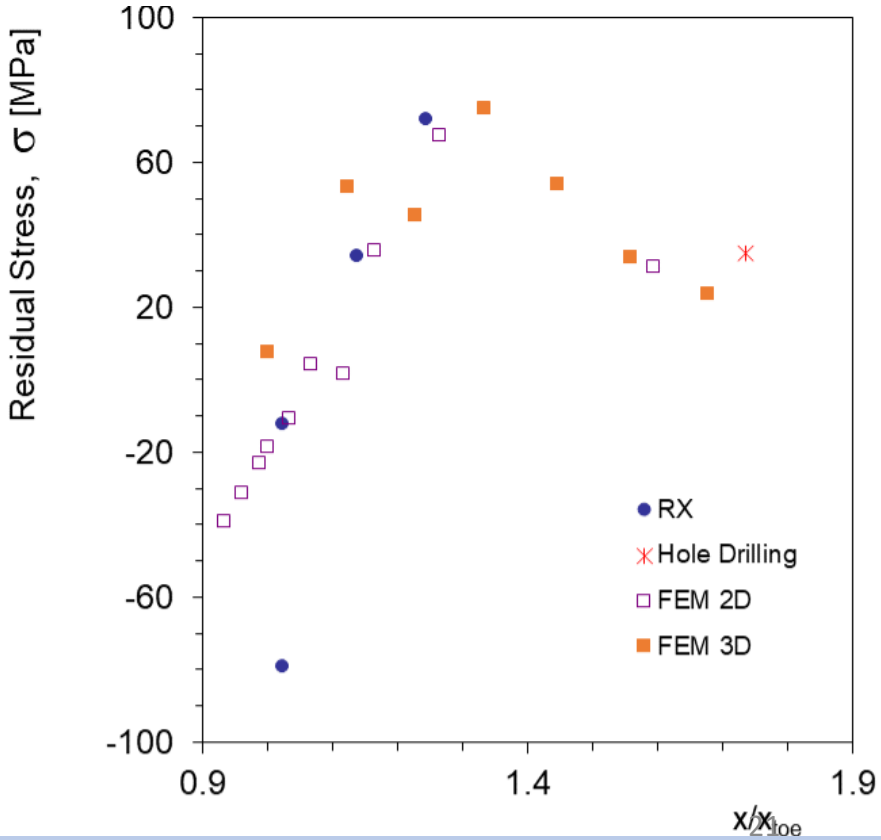

Results Discussion – Numerical analysis

- In table are presented the estimated lives of the TR-D specimen, where the TIG remelting conduces to the integral repair of pre-existing fatigue cracks with depths lesser than 2.5 mm;
- $N_{estimated}$ and $N'_{estimated}$ correspond respectively to the lives obtained at the simulations with and without the initial condition of stress field generated by TIG dressing;
- $\Delta\sigma$ corresponds to the nominal stress range at the weld toe.

Table – Fatigue simulations for TR-D specimen.

a_r [mm]	$\Delta\sigma$ [MPa]	$N_{exper.}$	$N_{estimated}$	$N'_{estimated}$	Estimated fracture surface
<2.5	352.6	628739	572837	531627	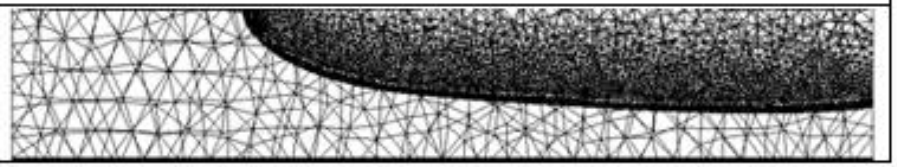

Results Discussion – Numerical analysis

- In table are presented the same results for the TDR3 specimen where the TIG remelting conduces to the poor repair of pre-existing fatigue crack with the depth of 4.8 mm;
- The TIG remelting produces an approximately semi-elliptic embedded crack with the depth of 3.3 mm and the length of 30 mm.

Table – Fatigue simulations for the TDR3 specimen.

a_r [mm]	$\Delta\sigma$ [MPa]	$N_{exper.}$	$N_{estimated}$	$N'_{estimated}$	Estimated fracture surface
4.80	204.7	361890	391110	322299	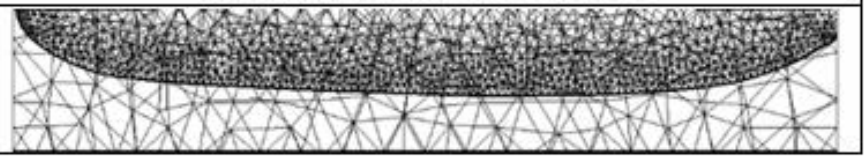

Results Discussion – Numerical analysis

- The videos show the evolution of the crack front along the simulations

TR-D specimen

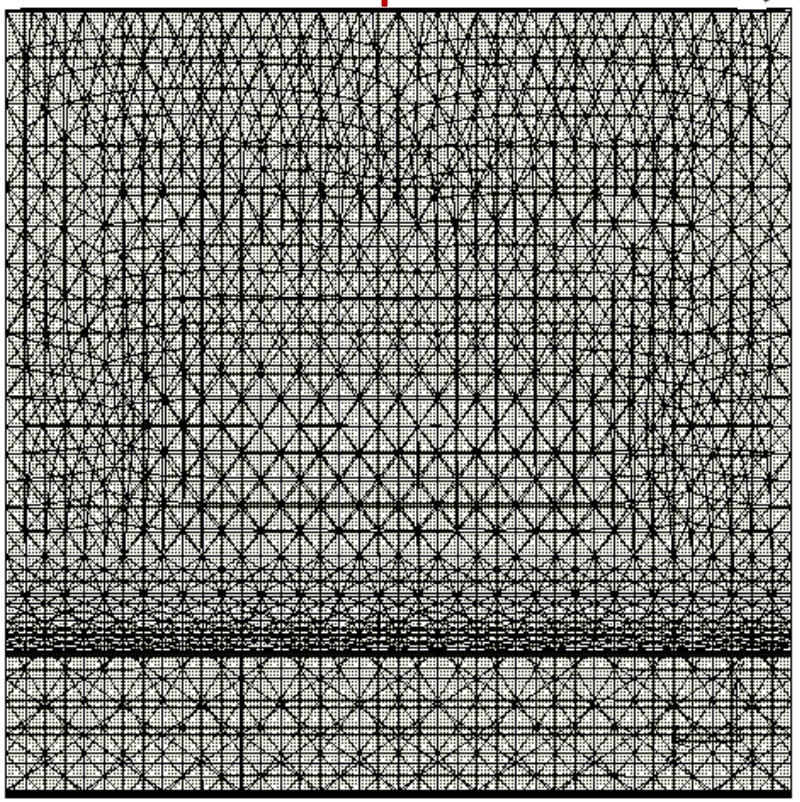

TR3 specimen

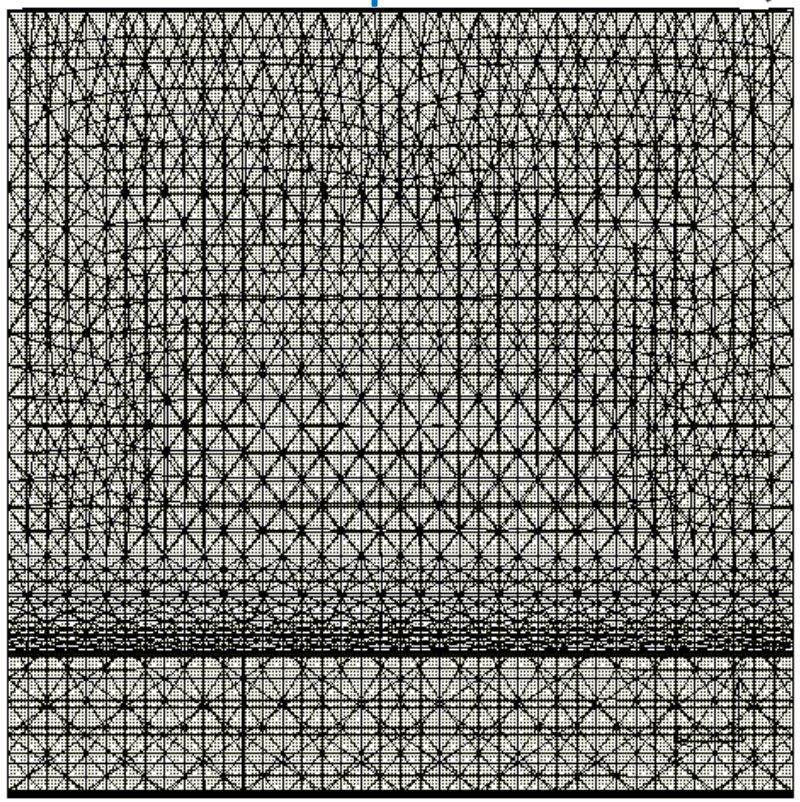

Results Discussion – Numerical analysis

From the presented numerical results, we can draw the following considerations:

- The estimated lives for TR-D specimen with and without initial stress fields present a deviation from the experimental one of 9% and 15%, respectively;
- The estimated lives for TDR3 specimen with and without initial stress fields, both present a deviation of 11% to the experimental one, the first by excess and the second by default;
- The numerical model produces a good estimation of the experimental life of the specimens;
- The estimated geometry for the final configuration of the crack is close to what occurs in the specimens;
- The compression stress field generated by TIG dressing causes a delay in crack growth.

Conclusions

- TIG remelting is a good rehabilitation technique for welded joints with shallow cracks (up to 2.5 mm depth) at the weld toe, contributing significantly to fatigue life extension;
- The use of TIG remelting as a fatigue crack repair technique must be associated with an adequate monitoring technique to ensure that the repair is carried out at an early stage of propagation, when the cracks are still shallow;
- Plasma remelting in the keyhole variant promotes a reasonable fatigue live recovery in the repair of deep cracks, however due to a pore density generated very high, is not acceptable as a rehabilitation technique for welded joints;
- The developed 3D Finite Element Model reveals to be effective to predict the growth of cracks at the weld toe of a T-joint;
- This Model reveals to be effective to evaluate the influence of residual stresses generated by the TIG remelting process at the weld toe, on the crack propagation speed;
- This Model reveals to be effective to predict the growth of embedded cracks resulting from poor repairs.

Thank You!

- **Main References**

Goldak, J., Chakravarti, A., Bibby, M., 1984. A New Finite Element Model for Welding Heat Sources. Metallurgical Transactions B, 15B: 299-305.

S. Manteghi and S.J. Maddox. Methods for fatigue life improvement of welded joints in medium and high strength steels. IIW Doc. XIII-2006-04 (2004).

A. Manai. An analysis of pre-fatigued TIG-treated welded structures. Engineering Failure Analysis (2021) 121: 105150.

J. Hedegård, M. Al-Emrani, M. Edgren, A. Manai, H. Al-Karawi, Z. Barsoum. LifeExt – Prolonged life for existing steel bridges. Open report (2020), DOI: 10.13140/RG.2.2.24449.99681.

C.M. Branco, V. Infante, R. Baptista. Fatigue behaviour of welded joints with cracks, repaired by hammer peening. Fatigue Fract Eng Mater Struct (2004) 27(9):785–98.

R.J. Dexter and J.M. Ocel. Manual for Repair and Retrofit of Fatigue Cracks in Steel Bridges. Tech. rep. No. FHWA-IF-13- 020, United States. Federal Highway Administration (2013).

A. Manai. A framework to assess and repair pre-fatigued welded steel structures by TIG dressing. Engineering Failure Analysis (2020) 118: 104923.

A.L. Ramalho, A.L., J.A.M. Ferreira, C.M. Branco. Fatigue Behaviour of T Welded Joints Rehabilitated by Tungsten Inert Gas and Plasma Dressing. Materials and Design (2011) 32:10, 4705-4713.

A.L. Ramalho, F. Antunes, J.A.M. Ferreira. Caraterização Mecânica do Aço S 355 a Temperatura Elevada, TEMM2018 – 1st Iberic Conference on Theoretical and Experimental Mechanics and Materials, 4-7 November 2018, Porto, Portugal.

A.L. Ramalho, F. Antunes, J.A.M. Ferreira. Crack Growth In Simulated Residual Stress Fields On Tungsten Inert Gas Dressed Welded Joints – A 2D Approach. Anales de la Mecânica de la Fractura (2020), 104-109.

A.L. Ramalho, F. Antunes, J.A.M. Ferreira. Simulation of crack growth in T-welded joints - residual stress field effect. Procedia Structural Integrity (2021) 33: 320–329.